

Spatial and temporal characteristics of droughts in Luanhe River basin, China

Yixuan Wang¹ · Ting Zhang¹ · Xu Chen¹ · Jianzhu Li¹ · Ping Feng¹

Received: 3 May 2016 / Accepted: 19 January 2017
© Springer-Verlag Wien 2017

Abstract The spatial and temporal characteristics of drought are investigated for Luanhe River basin, using monthly precipitation data from 26 stations covering the common period of 1958–2011. The spatial pattern of drought was assessed by applying principal component analysis (PCA) to the Standardized Precipitation Index (SPI) computed on 3- and 12-month time scales. In addition, annual SPI and seasonal SPIs (including spring SPI, summer SPI, autumn SPI, and winter SPI) were also defined and considered in this study to characterize seasonal and annual drought conditions, respectively. For all seven SPI cases, three distinctive sub-regions with different temporal evolutions of droughts are well identified, respectively, representing the southeast, middle, and northwest of the Luanhe River basin. The Mann-Kendall (MK) trend test with a trend-free pre-whitening (TFPW) procedure and Sen's method were used to determine the temporal trends in the annual and seasonal SPI time series. The continuous wavelet transform (CWT) was employed for further detecting the periodical features of drought condition in each sub-region. Results of MK and Sen's tests show a general tendency of intensification in summer drought over the entire basin, while a significant mitigating trend in spring drought. On the whole, an aggravating trend of inter-annual drought is discovered across the basin. Based on the CWT, the drought variability in the basin is generally dominated by 16- to 64-month cycles, and the 2- to 6-year cycles appear to be obvious when concerned with annual and seasonal droughts. Furthermore, a cross wavelet analysis

was performed to examine the possible links between the drought conditions and large-scale climate patterns. The teleconnections of ENSO, NAO, PDO, and AMO show significant influences on the regional droughts principally concentrated in the 16- to 64-month period, maybe responsible for the physical causes of the cyclical behavior of drought occurrences. PDO and AMO also highlight a noteworthy correlation with drought variability on a decadal scale (around 128-month period). The findings of this study will provide valuable references for regional drought mitigation and water resource management.

Keywords Drought · Spatio-temporal variability · Wavelet analyses · Large-scale climate cycles

1 Introduction

Drought is not only a natural phenomenon but also a devastating disaster worldwide (Lorenzo-Lacruz et al. 2010; Ujeneza and Abiodun 2015). Drought commonly starts with a shortage of precipitation over an extended period of time, and its occurrence and evolution are controlled by many factors which are dependent on the atmosphere and the hydrologic processes (Mishra and Singh 2010; Li et al. 2013a). The distribution and characteristics of droughts are highly irregular in both spatial and temporal dimensions (Wu et al. 2008; Potop and Soukup 2009). Therefore drought conditions with complex physical causes are more difficult to identify and assess than other natural hazards (Paulo et al. 2012; Hosseinzadeh Talaei et al. 2014).

A variety of indices have been developed with the objective of detecting and monitoring droughts (Heim 2002; Mishra and Singh 2010; Vicente-Serrano et al. 2012). The Standardized Precipitation Index (SPI) developed by McKee et al. (1993)

✉ Ting Zhang
zhangting_hydro@tju.edu.cn

¹ State Key Laboratory of Hydraulic Engineering Simulation and Safety, Tianjin University, Tianjin 300072, China

has become the most widely used drought index due to its computational simplicity and versatility (Bonaccorso et al. 2003; Livada and Assimakopoulos 2007; Edossa et al. 2010). The SPI, simply the standard normal value, is transformed from precipitation time series in a probabilistic manner. It can be calculated at varying time scales and permits to compare drought severity across time and space. The multi-scale strength allows SPI to monitor meteorological and agricultural drought at shorter time scale (1–3 months), as well as hydrological and water resource droughts at longer time scales (e.g., 6 and 12 months) (McKee et al., 1995; Szalai et al., 2000; Paulo and Pereira, 2006).

Nowadays, there seems to be a consensus about the fact that global warming results in increases in the frequency, duration, and severity of droughts at regional scales and the strong evidence for the exacerbating effects of intensified human activities (e.g. Wen et al. 2011; Russo et al. 2013; Li et al. 2013a). In this content, the spatial and temporal variability of droughts is anticipated to be more significant, leading to a higher risk of drought and more difficulties in water resource planning and management. Thus, it is necessary to realize how drought conditions vary in time and space at a regional scale. Accordingly, a large number of hydrologists worldwide have evaluated the spatial and temporal patterns of droughts using drought indices and statistical methods (such as principal component analysis (PCA) and cluster analysis (Santos et al. 2010; Martins et al. 2012; Capra and Scicolone 2012; Wang et al. 2015a), continuous wavelet transform (CWT) (Liu et al. 2013; Li et al. 2013b), Mann-Kendall (MK) trend test (Vargas et al. 2011; Vicente-Serrano et al. 2014), Sen's slope estimator (Gocic and Trajkovic 2013; Da Silva et al. 2015), and Fourier analysis (Moreira et al., 2015).

In recent years, the correlations between regional droughts and large-scale atmospheric circulation patterns have received significant attention. Considerable researches have revealed that the evolution of droughts in time and space can be explained in terms of climate anomalies such as the El Niño Southern Oscillation (ENSO), the North Atlantic Oscillation (NAO), and the Atlantic Multidecadal Oscillation (AMO) and the Pacific Decadal Oscillation (PDO) (e.g., Özger et al. 2009; Yin et al. 2009; Chen et al. 2013; Oglesby et al. 2012; Zhang et al. 2013). Several studies have provided evidence of noticeable associations between the large-scale climate oscillations and drought variability in northern China. For example, Ma (2007) pointed out that warm (cold) PDO phases favor drought (wet) conditions in North China by using correlation analysis. Su and Li (2012) analyzed possible teleconnections between large-scale climate indices and drought occurrences during 1868–2010 in Beijing which is located in northern China and found

significant correlations between the drought occurrences and four climate patterns (Arctic Oscillation (AO), ENSO, NAO, and PDO). Wang et al. (2015b) investigated effects of large-scale climate patterns on hydrological drought at different time scales over Luanhe River basin, China, indicating significant linkages of ENSO and AMO to the drought conditions. The cross wavelet analysis, a bivariate extension of wavelet analysis with several appealing qualities, is proven to be a useful tool to study the relationships between two time series in hydrology, contributing to the identification of forcing mechanisms (Schaeffli et al. 2007; Özger et al. 2009; Labat 2008; Labat 2010). Hence, to better understand the drought teleconnections in response to large-scale climatic patterns, the cross wavelet analysis is expected to provide relevant information.

This study focuses on the Luanhe River basin located in North China, which is of great importance for water supply to Tianjin city. The Luanhe River basin is a semi-arid and semi-humid area with a vulnerable eco-environment. During the last decade, it is observed that the area has experienced more frequent and more intensive droughts, resulting in diminished water resource availability and reduced carrying capacity of the ecosystems (Li and Feng 2007; Gao 2012; Wang et al. 2015b). In addition to climate changes, the growing water demands caused by population increase and the rapid development of economics and society are continuing to aggravate this deteriorating condition (Ma et al. 2010; Wang et al. 2013). The characterization of the spatial and temporal variability of the droughts can be very useful for an adequate water resource management at regional scale. Several studies have been undertaken to depict the drought characteristics in the Luanhe River basin (e.g., Ma et al. 2013; Yang et al. 2013). However, a comprehensive assessment of spatial and temporal patterns of droughts in the Luanhe River basin is still lacking. Moreover, the detailed links between large-scale climate anomalies and regional droughts are seldom investigated, calling for more studies to understand the atmospheric dynamics that modulate drought occurrence and severity over the region.

On these grounds, the main goal of the present research is to systematically determine the spatial and temporal characteristics of drought condition over the Luanhe River basin. Specifically, this study intends (1) to identify sub-regions characterized by distinct drought behaviors using the PCA with varimax rotation and the SPI at various time scales; (2) to detect temporal trends and periodical features of droughts in the identified sub-regions by the MK trend test with a trend-free pre-whitening (TFPW) procedure, the Sen's slope estimator and the CWT; and (3) to investigate the possible association of the individual drought variability with large-scale climate indices applying the cross wavelet analysis.

2 Study area and data

2.1 Study area

Luanhe River basin is located on the northern part in the Haihe River basin, China (Fig. 1), largely defined by 115° 30' E to 119° 15' E longitude and 39° 10' N to 42° 30' N latitude. It is about 33,700 km² in drainage area, in which mountainous regions account for nearly 98% with the rest 2% as plains. The topography of the basin significantly descends from northwest to southeast, along with the elevation ranging from 2205 to 2 m. This basin has a typical temperate continental monsoon climate. Its average temperature and average potential evapotranspiration are around -0.3–11 °C and 950–1150 mm/year, respectively. The amount of precipitation within the basin is unevenly distributed in both time and space. The mean annual precipitation varies from less than 400 mm, in the northwest, to more than 700 mm, in the southeast. About 70–80% of the annual precipitation is received during the period of June to September, which exhibits a high seasonal variability.

The Luanhe River basin bears the heavy responsibility of water supply for Tianjin city, the largest opening coastal city in North China. However, the basin has witnessed serious drought events with high intensity and prolonged duration in recent years, such as multi-year droughts for 1980–1984 and the consecutive drought during 1997–2005 (Li and Feng 2007; Ma et al. 2013; Yang et al. 2013). The frequent and severe droughts have inflicted devastating impacts on socio-economic development and eco-environment of the basin and have further deteriorated water resources availability in the Tianjin city. Thus, an improved understanding of the spatial and temporal behavior of droughts is of paramount importance to formulating a regional water resources management strategy.

2.2 Data

In this study, 54 years (January 1958 to December 2011) of monthly precipitation data was collected from 26 rain-gauging stations in the Luanhe River basin. The original dataset were provided by Hydrology and Water Resource Survey Bureau of Hebei Province. There were a few missing precipitation data in the dataset, and they were estimated by using linear regression equations which were fitted to the available monthly data observed at the station and at a nearby reference station (Bonaccorso et al. 2003; Vicente-Serrana 2006). As shown in Fig. 1, the 26 stations represent a good spatial coverage over the study area. Some information related to the selected stations (including location, elevation, and annual average precipitation) are provided in Table 1.

The Southern Oscillation Index (SOI) is a standardized index based on the observed sea level pressure differences

between Tahiti and Darwin, Australia, used for measuring the large-scale fluctuations in air pressure occurring between the western and eastern tropical Pacific during El Niño and La Niña episodes. The monthly data covering the period 1951–2015 is downloaded from the website (<http://www.cpc.ncep.noaa.gov/data/indices/soi>).

The North Atlantic Oscillation (NAO) is one of the most prominent teleconnection patterns in all seasons (Barnston and Livezey 1987). The NAO index is based on the surface sea level pressure difference between the subtropical (Azores) high and the subpolar low. Time series data for monthly mean NAO index from 1950 to 2015 is downloaded from the website (<http://www.cpc.ncep.noaa.gov/products/precip/CWlink/pna/nao.shtml>).

The Pacific Decadal Oscillation (PDO) is a shift in the temperature pattern of the North Pacific Ocean which occurs on a 20- to 30-year cycle. The PDO Index is defined as the leading principal component of North Pacific monthly sea surface temperature variability, available monthly from 1900 to 2015 in the website (<http://research.jisao.washington.edu/pdo/PDO.latest>).

The Atlantic Multidecadal Oscillation (AMO) is the long time scale variability of sea surface temperatures in North Atlantic with a 65–80-year cycle (Kerr 2000). The AMO index is defined as the detrended, regionally averaged, summer sea surface temperature anomalies over the North Atlantic Ocean (0–60° N, 7.5–75° W) (Enfield et al. 2001). The monthly AMO index from 1856 to 2015 is downloaded from the NOAA Earth System Research Laboratory (http://www.esrl.noaa.gov/psd/gcos_wgsp/Timeseries/AMO).

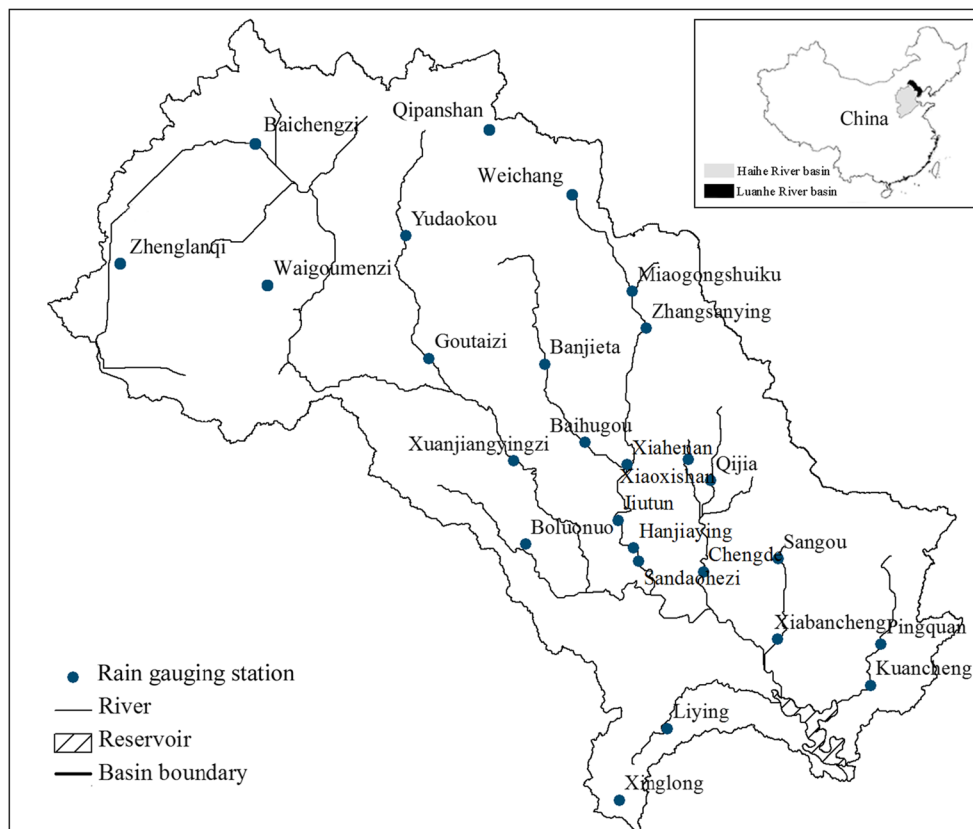
3 Method

3.1 Standardized precipitation index

The Standardized Precipitation Index (SPI) developed by McKee et al. (1993, 1995) has become the most popular drought index because of its simple calculation, robustness, and versatility. As a probability-based and standardized index, the SPI is spatially invariant in its interpretation, allowing comparison across different locations within the same region (Guttman 1997; Bordi et al. 2004; Vicente-Serrano et al. 2014).

Moreover, the SPI has the capability to monitor drought conditions over various time scales, facilitating impact assessments of both short- and long-term drought. Generally, the SPI calculated at 1 month is considered as a meteorological drought index (Hayes et al. 1999). The SPI on a shorter time scale (3 or 6 months) is adequate for depicting drought events affecting agricultural practices, while on longer time scales (12 or 24 months), it can better replicate hydrological and water resource droughts, important to water supply

Fig. 1 Location of the Luanhe River basin and the 26 rain-gauging stations



management interests (Vicente-Serrano and López-Moreno 2005; Paulo and Pereira 2006; Mishra and Singh 2010).

For a given location and an individual month, the SPI at w-month time scale (represented as SPI_w in this study) is calculated based on the running series of precipitation accumulated over w months. According to McKee et al. (1993), a two-parameter gamma distribution is used for fitting the empirical probability distribution of the accumulated precipitation. The fitted cumulative distribution is then transformed into a standardized normal distribution by employing the approximate

conversion provided by Abramowitz and Stegun (1965). The standardized normal variables (with zero mean and unit variance) are the values of SPI_w. Positive SPI values indicate wet conditions, and negative values indicate dry conditions.

In this study, the SPI index is also defined annually for each season and for the hydrological years of 1958–1959 to 2010–2011. For the Luanhe River basin, spring is from March to May, summer is from June to August, autumn is from September to November, winter is from December to February, and hydrological year is from June to May of the

Table 1 Detailed information about the 26 rain-gauging stations

Station	Location		Ele (m)	AP (mm)	Station	Location		Ele (m)	AP (mm)
	E	N				E	N		
Yudaokou	116° 58'	42° 02'	1400	420.33	Xinglong	117° 29'	40° 25'	620	525.46
Zhenglanqi	116° 01'	42° 11'	1360	355.1	Qijia	118° 06'	41° 27'	610	539.02
Waigoumenzi	116° 37'	41° 51'	1250	418.98	Pingquan	118° 42'	40° 59'	540	522.36
Baichengzi	116° 28'	42° 17'	1230	334.3	Bolounuo	117° 18'	41° 05'	540	513.07
Banjietia	117° 30'	41° 52'	1070	449.48	Xiahenan	117° 42'	41° 18'	520	513.22
Goutaizi	117° 05'	41° 33'	980	472.33	Hanjiaying	117° 50'	40° 56'	490	502.35
Qipanshan	117° 40'	42° 01'	950	465.57	Xiaoxishan	117° 56'	41° 11'	490	510.12
Miaogongshuiku	117° 50'	41° 43'	940	514.92	Sandahezi	117° 42'	40° 58'	460	517.88
Weichang	117° 46'	41° 54'	870	449.43	Sangou	118° 15'	41° 02'	430	524.14
Jiutun	117° 23'	41° 17'	850	521.06	Liyong	117° 44'	40° 36'	420	637.29
Xuanjiangyingzi	116° 52'	41° 23'	830	502.68	Chengde	117° 56'	40° 58'	350	512.01
Baihugou	117° 26'	41° 34'	830	486.68	Xiabancheng	118° 10'	40° 47'	350	546.2
Zhangsanying	117° 45'	41° 34'	640	493.18	Kuancheng	118° 30'	40° 37'	300	636.81

Note: “Ele” means elevation, and “AP” means annual average precipitation

subsequent year. Let $P(t)$ represent the precipitation measured at time t ($\Delta t = 1$ month in this study). The series $P(t)$ is subdivided into 12 smaller series $P^m(y)$, one for each month, in which $m = 1$ (Jan), 2 (Feb), ..., 12 (Dec) is the month index, y is the year index, and the time index $t = 12(y - 1) + m$. Considering the 54 years (January 1958 to December 2011) of monthly precipitation data used in this study, the year index $y = 1958, 1959, \dots, 2011$. Therefore, $P^{\text{Jan}}(1958)$ represents January precipitation in 1958, and $P^{\text{Dec}}(2011)$ represents December precipitation in 2011. The precipitation accumulated in spring is expressed as $P^{\text{Spr}}(y) = P^{\text{Mar}}(y) + P^{\text{Apr}}(y) + P^{\text{May}}(y)$. The procedure of spring SPI (SPI_{spr}) calculation involves fitting a two-parameter gamma distribution to the time series of cumulative precipitation in spring ($P^{\text{Spr}}(y)$). According to the approximate conversion (Abramowitz and Stegun 1965), the cumulative probability of P^{Spr} is then transformed to the standard normal deviation, which is the value of SPI_{spr} . Thus, $\text{SPI}_{\text{spr}}(y)$ is the annual series of spring SPI, where $y = 1958, 1959, \dots, 2011$. Analogously, the summer SPI (SPI_{sum}) and the autumn SPI (SPI_{aut}) are defined as the SPI calculated based on the 3-month cumulative precipitation series for summer and autumn ($P^{\text{Sum}}(y)$ and $P^{\text{Aut}}(y)$) respectively, where $y = 1958, 1959, \dots, 2011$. The cumulative precipitation in winter is calculated by $P^{\text{Win}}(y) = P^{\text{Dec}}(y) + P^{\text{Jan}}(y + 1) + P^{\text{Feb}}(y + 1)$, and consequently, the winter SPI (SPI_{win}) series covers the period of 1958–2010. The annual SPI (SPI_{ann}) is calculated based on the time series of the 12-month precipitation total from June to May in the next year (namely the precipitation accumulated in the whole hydrological year, $P^{\text{Ann}}(y) = P^{\text{Jun}}(y) + P^{\text{Jul}}(y) + \dots + P^{\text{Dec}}(y) + P^{\text{Jan}}(y + 1) + P^{\text{Feb}}(y + 1) + \dots + P^{\text{May}}(y + 1)$), where $y = 1958, 1959, \dots, 2010$. In doing so, the samples used for calculating the seasonal and annual SPI are collected annually and are subject to the same seasonal effect, consequently largely reducing the degree of auto-correlation among samples and appropriately accounting for the seasonal variation (Kao and Govindaraju 2010).

3.2 Principal component analysis

Principal component analysis (PCA) (Hotelling 1933), which is defined as a multivariate technique for dimensionality reduction, has been widely applied to identifying patterns in climatic data (e.g., Corte-Real et al. 1998; Raziqi et al. 2013; Gocic and Trajkovic 2014). The non-parametric PCA forms a set of new uncorrelated variables (named principal components or PCs scores) that are linear combinations of the original ones (Sharma 1996; Rencher 1998), effectively extracting useful information from huge or confusing datasets.

As to the standardized normalized variables (e.g., SPI data), the PCA method computes their covariance matrix and the corresponding eigenvalues and eigenvectors. The principal components are obtained from the projection of the original data onto the orthonormal eigenfunctions and are arranged in a

decreasing order according to the values of the associated eigenvalues. The eigenvectors, properly normalized, are the loadings that represent the weight of the original variables in the corresponding principal components, while their eigenvalues give information about the amount of variance explained by the components. Therefore, the first principal component corresponding to the largest eigenvalue explains the maximum possible variance of the original data, and the second principal component with the second highest eigenvalue explains as much as possible of remaining variance. An orthogonal rotation such as Varimax rotation is commonly applied to the calculated eigenvectors, so that the rotated principal components (RPCs) with a clearer division could provide more stable spatial patterns (Richman 1986). The rotated patterns preserve the orthogonality in time and simplify the spatial structure, thus producing more spatially localized loadings and increasing physical relevance and interpretation of the results (Kahya et al. 2008; Santos et al. 2010).

In this study, the rotated PCA were applied separately on the SPI at 3- and 12-month time scale, as well as the annual SPI and seasonal SPIs, to capture spatial patterns of drought over the Luanhe River basin. The quality of the PCAs was tested using the Bartlett's test of sphericity (Bartlett 1954) and the Kaiser-Meyer-Olkin (KMO) statistic (Kaiser 1970). The number of principal components retained for Varimax rotation was based on the criterion of an eigenvalue larger than 1. The rotated loadings were then mapped to identify sub-regions with independent drought variability, and the series of the associated RPC scores were used for representing temporal variability of drought condition for each sub-region.

3.3 Mann-Kendall trend test

The Mann-Kendall (MK) trend test (Mann 1945; Kendall 1975) is one of the mostly widely used non-parametric tests for trend detection in hydrologic time series. This test derived from a rank correlation test for two sets of observations requires only that the data be independent, and it is less sensitive to outliers in the data (Hamed 2008). Statistics in this test are distribution-free because they are depending only on the ranks of the observation.

Hydrological time series often display statistically significant serial correlation. The existence of serial correlation will increase the probability that the MK test detects a significant trend, and meanwhile, the presence of a trend will alter the estimate of the magnitude of serial correlation. In order to efficiently eliminate the influence of serial correlation on the MK trend test, the trend-free pre-whitening (TFPW) procedure proposed by Yue et al. (2002) was used in this study. This procedure involves first removing an identified trend from the sample data to obtain a detrended series, and then removing the lag 1 autoregressive (AR(1)) process from the detrended series to get an independent residual series. After

employing the TFPW procedure, the MK test is applied to the series which is the combination of the identified trend and the modified residual series. For a comprehensive introduction of the TFPW procedure, refer to Yue et al. (2002).

The MK test statistic Z is generally used to measure the degree to which a trend is consistently increasing or decreasing. Compared with the standard normal variate ($Z_{1-\alpha/2}$) at the desired significance level α , the significance of the trend is evident if $|Z| > |Z_{1-\alpha/2}|$, and the trend is not statistically significant otherwise. Details of the MK test, as well as the calculation of Z , can be found, e.g., in Gan (1998) and Kisi and Ay (2014).

3.4 Sen's slope estimator

Sen's slope produce developed by Sen (1968) is a simple non-parametric test for estimating the slope of trend in a sample. The Sen's method uses a linear model to determine the slope and calculates Sen's slope estimator (denoted by Q_{med}) to reflect data trend reflection. The value of Q_{med} indicates the steepness of the trend, and details of its calculation can be found in Sen (1968) and Da Silva et al. (2015). In the Sen's Method, single data errors or missing values are allowed, and the data need not conform to any particular distribution (Afzal et al. 2011; Yeh et al. 2015).

Sen's slope estimator has been widely used in hydro-meteorological time series (e.g., Partal and Kahya 2006; Tabari et al. 2011) and usually employed for identifying the true slope of MK trend analysis (Gilbert 1987; Kousari et al. 2013; Atta-ur-Rahman 2016). The Sen's produce applied following the MK test measures the magnitude of any significant trend found in the MK test. In this study, the MK and Sen's methods were used to determine whether there was an upward, downward, or no trend in SPI data with their statistical significance.

3.5 Wavelet analysis

Wavelet analysis is becoming a common method for analyzing the time series of hydro-meteorological variables in frequency domain (e.g., Ghil et al. 2002; Labat et al. 2004; Schaeffli et al. 2007; Labat 2008). It exhibits various advantages over the conventional Fourier method in preserving local, non-periodic, and multi-scaled features, thus providing a more powerful way for studying localized intermittent oscillations. What's more, the wavelet analysis is much preferred to the Fourier analysis because it is naturally dedicated to non-stationary signals.

The continuous wavelet transform (CWT) decomposes the time series into a superposition of stretched and translated versions of a mother wavelet with flexible resolution in both frequency and time, expecting to allow the completion of time scale representation of localized and transient phenomena occurring at different time scales. Compared with other mother

wavelet functions, the Morlet wavelet provides a good balance between time and frequency localizations and can well describe the shape of hydrological signals (Lafreniere and Sharp 2003; Labat et al. 2005).

In the present study, the continuous Morlet wavelet transform was used to establish a significant distinction between random fluctuations and periodic regions in the RPC scores. The characteristic periods of oscillation can be determined based on the wavelet power spectrum. Due to finite-length time series, the cone of influence (COI) was considered to highlight the region of the wavelet spectrum in which edge effects become important and the results should be ignored (Torrence and Compo 1998). To examine the statistical significance for wavelet spectrum, a background power spectrum was provided by a red noise model, and 95% confidence intervals were taken into consideration following Torrence and Compo (1998) calculations.

In addition, this study applied cross wavelet transform (XWT) and wavelet coherence (WCO) to examine the relationship between the RPC scores and large-scale climate indices. The XWT that constructed from two CWTs denotes their common power and relative phase in time-frequency space. The cross wavelet power spectrum defined by Torrence and Compo (1998) can be used for analysis of the covariance of two time series, with the statistical significance estimated against a red noise model. Following Torrence and Webster (1999), the WCO is defined as a useful measure of the intensity of the covariance. The cross wavelet power reveals areas with high common power, while the wavelet coherence is capable of finding significant coherence even though the common power is low. The statistical significance level of the coherence was determined using Monte Carlo methods with red noise (Jevrejeva et al. 2003). For a more complete introduction of wavelet analysis, refer to Grinsted et al. (2004), Maraun and Kurths (2004), and Labat (2005).

4 Results and discussion

4.1 Spatial pattern of droughts

The PCA was applied to the SPI field to delineate the drought spatial pattern of the Luanhe River basin. To reflect both short- and long-term drought conditions, monthly SPI series with 3- and 12-month time scales (SPI_3 and SPI_{12} , respectively) were calculated using the precipitation observations from 1958 to 2011 for the 26 selected stations. Concerned with seasonal and annual droughts which are of great interest to water resource managers, annual and seasonal SPIs (including SPI_{ann} , SPI_{spr} , SPI_{sum} , SPI_{aut} and SPI_{win}) were also calculated for all the stations at an annual time step. As previously mentioned, the length of each SPI series is equal to $53 \times 12 = 636$ for both the SPI_3 and SPI_{12} , and equal to 53 when referred to every

seasonal SPI or to the annual SPI (covering the period of 1958–2010). The KMO measures of sampling adequacy are 0.969, 0.908, 0.912, 0.890, 0.916, 0.876, and 0.875 with regard to the SPI₃, SPI₁₂, SPI_{ann}, SPI_{spr}, SPI_{sum}, SPI_{aut}, and SPI_{win} sets, respectively, indicating that these data sets are adequate for the PCA (KMO test statistic > 0.50). The Bartlett's tests of sphericity with the p value < 0.0001 ($\alpha = 0.05$) for all the sets also support the application of PCA.

The PCA results associated with all the considered SPI sets revealed only the first three principal components (PC) with eigenvalues larger than 1, and thus, the first three components for each SPI set were retained for Varimax rotation. The explained variances of un-rotated and varimax-rotated components for the seven SPI sets are summarized in Table 2. The percentage of variances explained by the first three PC is almost the same in all cases. In general terms, the cumulative total explained variances of the three retained PCs are about 80%, and the first three rotated principal components (RPC, hereafter F1, F2 and F3) account for approximately 39, 27, and 15% of the total variance, respectively.

The rotated loadings of the first three components are presented to show the most dominant patterns of drought condition in the study area. Figure 2 illustrates the spatial distribution of the rotated loadings over the Luanhe River basin for the seven SPI sets. A threshold value of 0.6–0.7 on the rotated loading is reasonable for spatially delimiting the sub-regions that experienced similar drought variability (blue areas in the maps) (Raziei et al., 2013). The spatial patterns of the rotated loadings with positive values for all the SPI sets are nearly identical, delineating northwest, middle, and southeast as three distinctive sub-regions within the Luanhe River basin, which are represented as R1, R2, and R3, respectively. The three sub-regions characterized by distinct drought variability are highly correlated with the associated RPC scores.

In the case of SPI₃ (Fig. 2(a)), the loading patterns corresponding to the F1 highlight 13 stations which are located in the southeastern part of the basin, showing high positive and spatial homogeneous correlation ($0.63 < r < 0.86$) between F1 score and drought variability in these stations. This sub-region (R1) with extensive urbanization and agriculture activity has lower elevation (around 450 m) and higher average annual precipitation (500–630 mm). Apparently, the F2 shows its high loadings with positive value larger than 0.62 at nine stations over the middle part which is mainly characterized by grassland and urban area. The mean elevation over this sub-region (R2) is about 800 m and the average annual precipitation is 450–540 mm. The F3 has relatively high positive loadings (>0.75) in the northwest including four stations. This sub-region (R3) is mostly forested with higher elevation (around 1300 m) and lower average annual precipitation (330–420 mm).

The spatial loading patterns of the RPC observed in the other SPI sets (SPI₁₂, SPI_{ann}, SPI_{spr}, SPI_{sum}, SPI_{aut}, and

SPI_{win}) coincide relatively well with those in SPI₃, showing that the three sub-regional drought patterns generally remain stable in their spatial homogeneity with different time scales. Thus, it is possible to conclude that the spatial structure of drought condition related with precipitation deficit seems to be well identified as three dominant sub-regions over the Luanhe River basin: the southeastern part (R1), the middle part (R2), and the northwestern part (R3). The temporal characteristic of SPI-based drought appears to be different on a sub-regional scale and depends on different precipitation regimes. Moreover, the similar spatial pattern obtained by SPI with various time scales makes valid to continue the further analysis based on one of those scales.

Generally, the four seasonal RPC sets have consistent spatial distributions with each other, but some marked differences derived from these seasonal patterns are worth noting. For example, the R2 sub-region identified by winter F2 is of relative small size than those identified by other seasonal RPCs, while the high loadings related to summer F2 determine the R2 sub-region covering a larger area. Moreover, the F3 of spring SPI accounts for 9% of the total spring drought variance, which is considerably below the average percentage (15%) of variances explained by the F3. Meanwhile, the relatively high loadings of the spring F3 is around 0.5, indicating that the R3 sub-region inferred by the spring F3 seems to be in-apparent. These inconsistencies among the spatial patterns of seasonal droughts suggest that different seasons may be controlled by different atmospheric circulations.

4.2 Temporal variability of droughts

4.2.1 Time series evolution

Due to the strong positive correlation between RPC scores and SPI series over the corresponding sub-region, the time series of RPC score can be serve as representative of the temporal variability of the sub-regional drought condition. Generally, the SPI with a longer time scale can filter out high frequency fluctuations and reserve the long-term behaviors, thus the time series of the first three RPC (F1, F2, and F3) scores for SPI₁₂ were selected to represent the drought evolution in the three identified sub-regions, illustrated in Fig. 3. Differences obviously emerge in the processes of the orthogonal RPC scores, showing the different temporal variability of drought over these sub-regions. The positive and negative values in all the RPC scores (representing wet and drought conditions, respectively) alternately appeared within the period of 1958–2011.

Over the R1 sub-region related to F1 score (Fig. 3a), the main severe droughts occurred in 1960–1962, 1971–1972, 1992–1993, 1999–2001, 2002–2003, and 2006–2007. This sub-region suffered several extreme droughts with the worst one in 1971–1972, which is in an agreement with the serious drought of 1972 recorded in history (Water Resources and

Table 2 Explained variances of the un-rotated and rotated principal components corresponding to seven SPI sets

PCs	SPI ₃		SPI ₁₂		SPI _{ann}		SPI _{spr}		SPI _{sum}		SPI _{aut}		SPI _{win}	
	UnR (%)	VR (%)	UnR (%)	VR (%)	UnR (%)	VR (%)	UnR (%)	VR (%)	UnR (%)	VR (%)	UnR (%)	VR (%)	UnR (%)	VR (%)
First PC	68.9	39.4	67.0	36.5	66.0	38.1	64.7	39.9	63.2	37.1	64.0	40.5	59.5	40.9
Second PC	8.4	25.6	8.2	26.2	7.7	26.1	14.6	34.7	7.9	27.7	10.7	27.6	13.8	24.4
Third PC	4.2	16.4	4.7	17.1	5.5	14.9	4.7	9.4	5.7	12.1	4.7	11.3	5.8	13.8
Cumulative	81.5	81.5	79.9	79.9	79.2	79.2	84.0	84.0	76.9	76.9	79.4	79.4	79.1	79.1

UnR un-rotated, VR varimax rotated

Hydropower Planning And Design General Institute, MWR, 2008). According to the F2 score series (Fig. 3b), the remarkable drought events with different severities are detected during the periods of 1963–1964, 1966–1968, 1983–1984, 1988–1990, 1995–1996, 2002–2003 and 2006–2007 in the R2 sub-region. The drought event in 1983–1984 identified with highest intensity is consistent with the consecutive drought in 1980–1984 which has already been reported by both Ma

et al. (2013) and Wang et al. (2015b). The R3 sub-region corresponding to F3 score experienced the major drought events in the periods 1975–1977, 1984–1985, 1989–1990, 1993–1994, 2000–2002, and 2007–2008 (Fig. 3c). The time series of F3 score appear to indicate intense drought episodes in the last decade and highlight a tendency towards drier conditions in this sub-region. This is in line with the conclusions reported by Wei and Feng (2011) and Wang et al. (2015c).

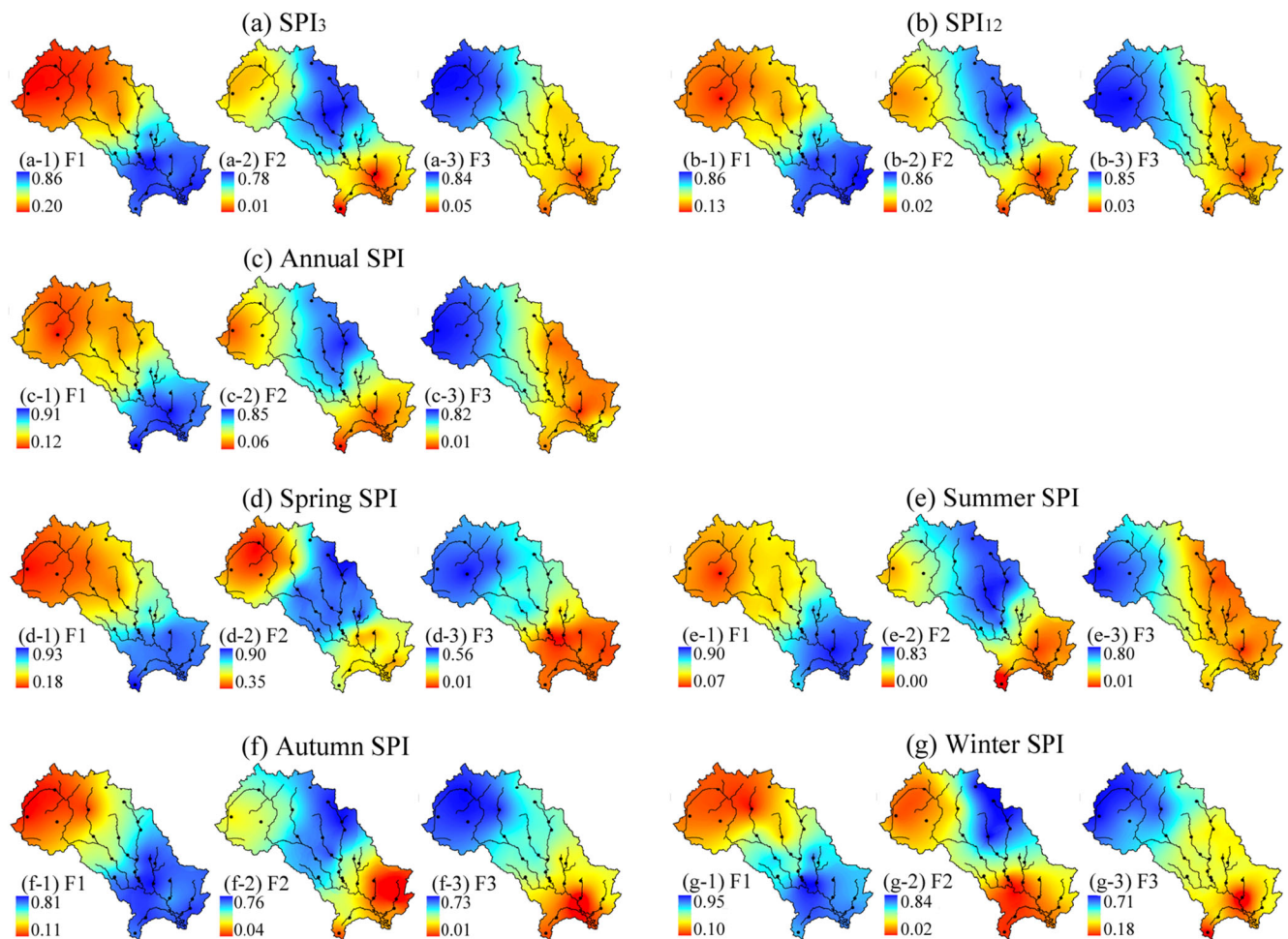


Fig. 2 Loading patterns of the first three rotated principal components (F1, F2, and F3) for the (a) SPI₃, (b) SPI₁₂, (c) annual SPI, (d) spring SPI, (e) summer SPI, (f) autumn SPI, and (g) winter SPI

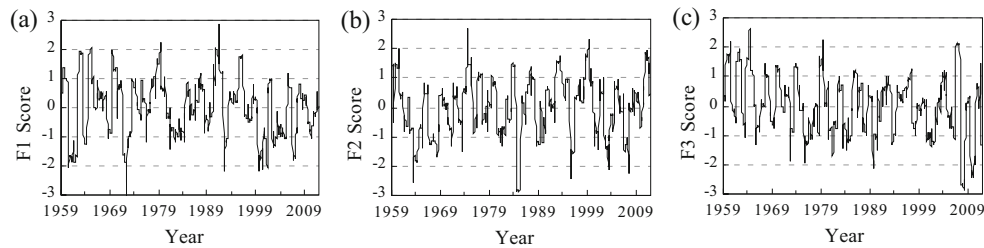


Fig. 3 Time series of the first three rotated principal components (a F1, b F2, and c F3) scores of the SPI field on 12-month time scale for the period 1958–2011

4.2.2 Trend detection

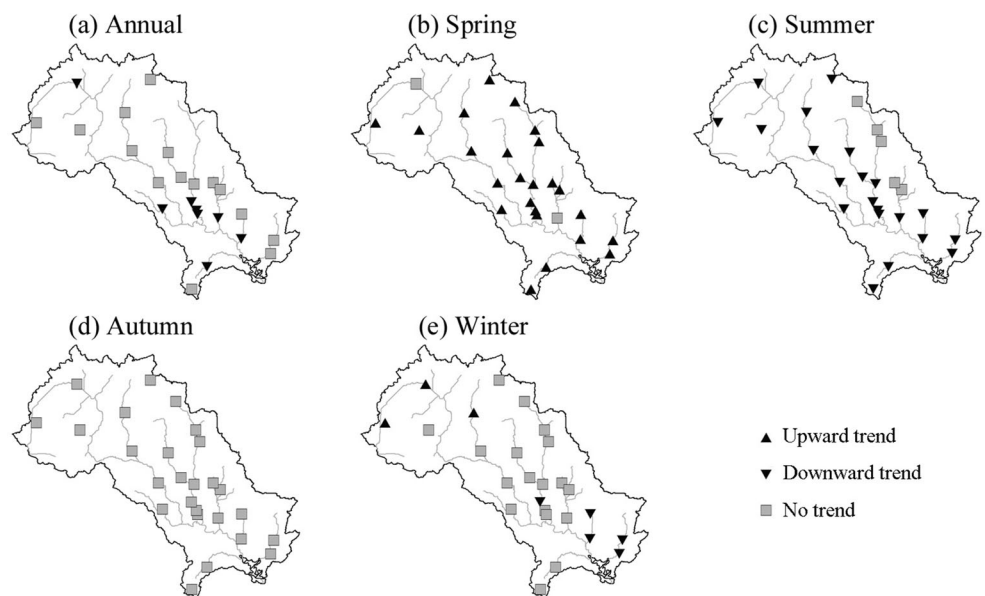
In order to detect the inter-annual trend of drought in the Luanhe River basin, MK test with the TFPW procedure and Sen’s method both at the 10% significance level were applied to the annual SPI series of 26 rain-gauging stations. Moreover, seasonal SPIs were also considered to account for the temporal trend at a seasonal scale. We determined whether there was an upward, downward, or no trend in the annual and seasonal SPI time series during the period 1958–2011 based on the statistic Z values of MK test and the Sen’s slope estimator (Q_{med}).

Spatial distributions of the rain-gauging stations with upward, downward, and no trends for the annual and seasonal SPI series were illustrated in Fig. 4. As for annual SPI (Fig. 4(a)), the significant downward trends were detected at the stations in southeast, while scarcely any significant upward or downward trends were found at the stations located in middle and northwestern parts. It is indicated that there seems to be an intensification of inter-annual droughts in the R1 sub-region, and

temporal tendency of annual drought is not evident in the R2 and R3 sub-regions.

The spring SPI had the significant upward trends at about 92% of stations (Fig. 4(b)), and the significant downward trends for summer SPI were presented at more than 80% of stations (Fig. 4(c)). It might imply that, on the whole, the drought condition in summer has a remarkable aggravating trend over the Luanhe River basin, while a mitigating trend is significantly identified for spring drought. These results agree with those of previous studies on the temporal analysis of droughts in the study area (Li and Zhou 2015; Wang et al. 2015c). However, as shown in Fig. 4(d), no significant upward or downward trend was identified in autumn SPI series, possibly suggesting that the magnitude of tendency change in autumn drought was low during the period of 1958–2011 in the study area. Moreover, a significant upward trend in winter SPI was found at the stations located in northwest, but a significant downward trend was observed at the stations in south-east (Fig. 4(e)). It appears to reveal an aggravating trend of winter drought in R1 sub-region while a mitigating trend in R3 sub-region.

Fig. 4 Spatial distribution of 26 rain-gauging stations with upward, downward, and no trends by the MK and Sen’s tests for the time series of annual and seasonal SPIs during the period 1958–2011 across the Luanhe River basin



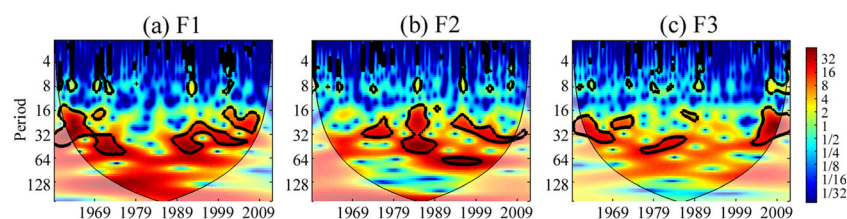


Fig. 5 Continuous Morlet wavelet power spectrum of time series of the first three rotated principal components (**a** F1, **b** F2, and **c** F3) scores for the SPI_{12} . The *thick black contours* depict the 5% significance level of

local power relative to red noise. The cone of influence (COI) where edge effects are not negligible is shown as a *lighter shade*

4.2.3 Periodic features of the RPC scores

The continuous wavelet transform (CWT) was further carried out to recognize the periodic cycles at the 5% significance level in the sub-regional SPI patterns which are represented by the time series of corresponding RPC scores. To leave securely off the effect of the seasonal cycle, the analysis of cyclical behavior based on the CWT in this study is concerned with the SPI data at 12-month time scale rather than SPI_3 . The wavelet power spectra (WPS) of the first three RPC (F1, F2, and F3) scores for SPI_{12} are presented in Fig. 5, showing that the SPI_{12} over the three main sub-regions are featured by different cycles with temporal variability in power.

The F1 score series related with the SPI_{12} in R1 sub-region exhibit 16- to 64-month cycles continuously possessing significant powers during the periods of 1961–1976 and 1988–2008, especially highlighting the 33- to 57-month cycles with relatively high powers (Fig. 5a). Although the wavelet powers of F1 show a reduced level of activity between these two periods, a considerable amount of power as 128-month cycle can be observed in the 1969–1989. The WPS of F2 score (Fig. 5b) suggest that the SPI_{12} over R2 sub-region generally has strong cycles of 16 to 64 months from 1971 to 2008. The 33- to 57-month and 61- to 75-month cycles show significant power during the 1980–1990 and the 1990–2000 respectively, indicating that these cycles may contribute remarkably to the frequent occurrence of severe droughts from 1980 to 2000 in the R2 sub-region. As for the WPS for F3 score (Fig. 5c), significant cycles of 18 to 40 months during the 1961–1974 are detected in the SPI_{12} in R3 sub-region, as well as the 33- to 57-month significant cycles during the 1976–1987. Moreover, 14- to 43-month cycles emphasize significant power from 2002 to 2010, appearing to account for the intensification of droughts over the R3 sub-region in recent decade.

In general, the drought variability of Luanhe River basin is dominated by 16- to 64-month cycles, but remarkable differences are observed in the cyclic structures related to the three main sub-regions, further confirming that the temporal characteristics of these sub-regions are different from each other. Due to the shortness of the available data, the periodical features obtained in this study remain restricted to inter-annual and inter-decadal scales. The localized intermittent periodicities discovered by CWT can provide useful information for

the regional drought risk analysis, and they will be conducive to better understanding the atmospheric dynamics that modulate drought occurrence and severity on a sub-regional scale.

To further detect the periodic features of annual and seasonal droughts in the three main sub-regions, the CWT was also applied to the first three RPC scores corresponding to annual and seasonal SPI sets. For the annual F1 score, the WPS (Fig. 6(a-1)) are observed in 95% confidence regions mainly during 1961 to 1976 at the 2- to 4-year scale and during 1971 to 1978 at the 10- to 13-year scale. The WPS for annual F2 score (Fig. 6(a-2)) show 2.5- to 4.5-year cycles having significant powers during the periods of 1984–1987 and 2000–2006, as well as 5- to 6.5-year cycles during 1989–1999. In addition, the WPS of annual F3 score (Fig. 6(a-3)) present non-significant but strong cycles of 2.5 to 4 years from 1980 to 1985. It is suggested that the annual drought of the Luanhe River basin is mainly characterized by 2- to 6-year cycles, which is consistent with the CWT results of SPI_{12} . As for all the seasonal SPIs, their first three RPC scores mostly detected significant wavelet powers at the 2- to 6-year scale, while the specific cyclic patterns vary from season to season and differ depending upon the sub-region identified (Fig. 6(b)–(e)). These results corroborate that the main drivers of the periodical features of seasonal droughts seem to be related with different oscillations in global climate system. The dominant factors also change spatially over the Luanhe River basin, generating the three identified sub-regions with individual temporal evolution of drought conditions.

4.3 Links between global teleconnections and sub-regional droughts

Considering the teleconnections of ENSO, NAO, PDO, and AMO, the cross wavelet transform (XWT) and wavelet coherence (WCO) were utilized to detect common properties and correlations between the climate indices and the sub-regional drought signals which are represented by the first three RPC (F1, F2, and F3) scores for SPI_{12} . The detections were performed above the 5% significance level along with more focus on inter-annual and decadal scales.

The cross wavelet power spectrum and wavelet coherence between the F1 score and each climate index in 1958–2011 are shown in Fig. 7. The results indicate that the drought

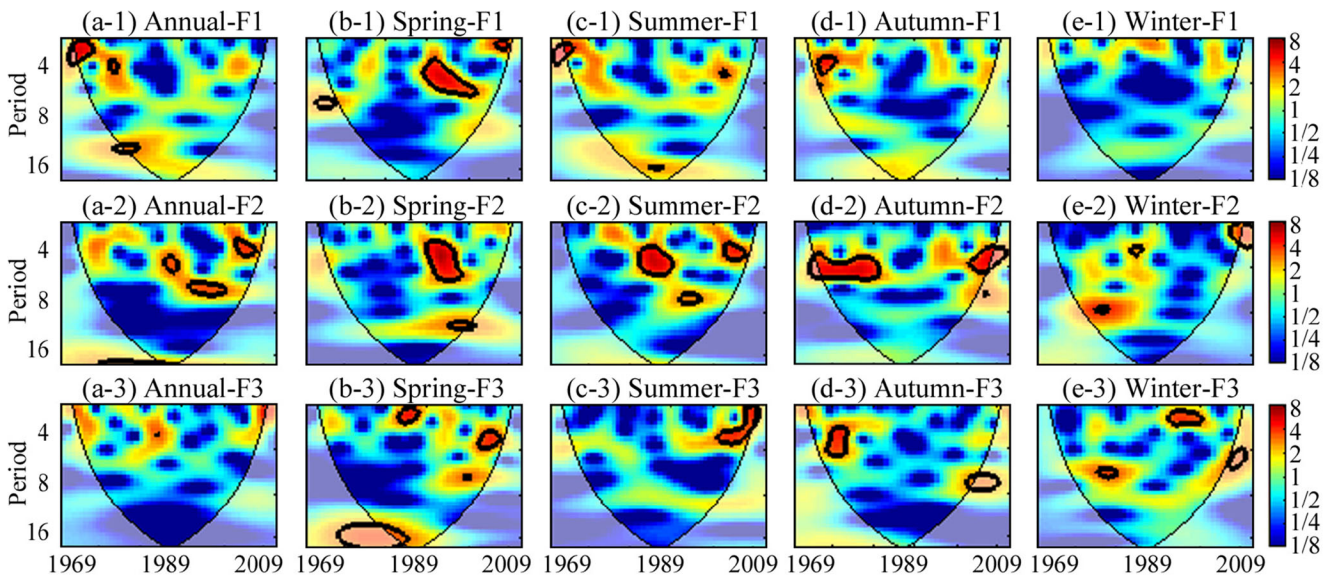


Fig. 6 Continuous Morlet wavelet power spectrum of time series of the first three rotated principal components (a) F1, (b) F2 and (c) F3 scores for the SPI_{ann} , SPI_{spr} , SPI_{sum} , SPI_{aut} , and SPI_{win} . The thick black contours

depict the 5% significance level of local power relative to red noise. The cone of influence (COI) where edge effects are not negligible is shown as a lighter shade

variability in R1 sub-region has a statistically significant correlation with SOI in the 18- to 57-month period from 1969 to 1977 and in the 66- to 75-month period from 1993 to 2004. NAO with 18–33-month period signals shows the most significant influence on F1 during 1960–1975, and PDO with 37–50-month period signals in 1970–1974 as well as 57–66-month period signals in 1988–1997 shows a remarkable influence. AMO exhibits significant correlations with the F1 score in the 33- to 57-month period during 1969–1975 and in the 14- to 37-month period during 1993–2003. Moreover, a noteworthy association between the sub-regional drought and AMO is detected for the period 1973–2001 at a decadal scale (100- to 130-month period).

For the drought variability in R2 sub-region, the results of cross wavelet analysis are presented in Fig. 8, suggesting a

significant correlation with SOI in the 25- to 33-month period from 1970 to 1977 and in the 37- to 75-month period from 1984 to 1998. There is also a significant correlation with NAO in the 37- to 43-month period from 1983 to 1987 and in the 16- to 32-month period from 1999 to 2004. The variation in F2 score is closely related to the PDO associated with 57–76-month signals during 1965–1975, 14–37-month signals in both the periods of 1975–1980 and 1993–2009, and signals on the 33–43 and 66-month scales during 1980–1986. AMO also shows substantial influence on F2 in the 33- to 57-month period from 1980 to 1990.

As shown in Fig. 9, the drought variability in R3 sub-region is poorly linked with the teleconnection of ENSO (depicted with the SOI index) at the scale large than 1 year, while the strong influence of NAO is clearly seen in the 28- to

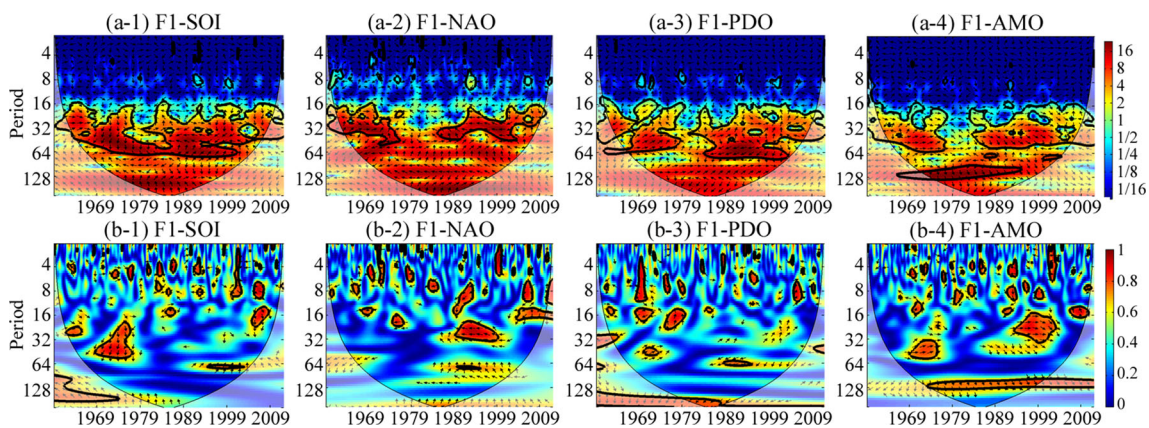


Fig. 7 **a** Cross wavelet power spectrum and **b** wavelet coherence between F1 score series of SPI_{12} and climate indices (SOI, NAO, PDO, and AMO). The thick black contours depict the 5% significance level of

local power relative to red noise, and the cone of influence (COI) is shown as a lighter shade. Right-pointing arrows indicate that the two signals are in phase while left-pointing arrows are for anti-phase signals

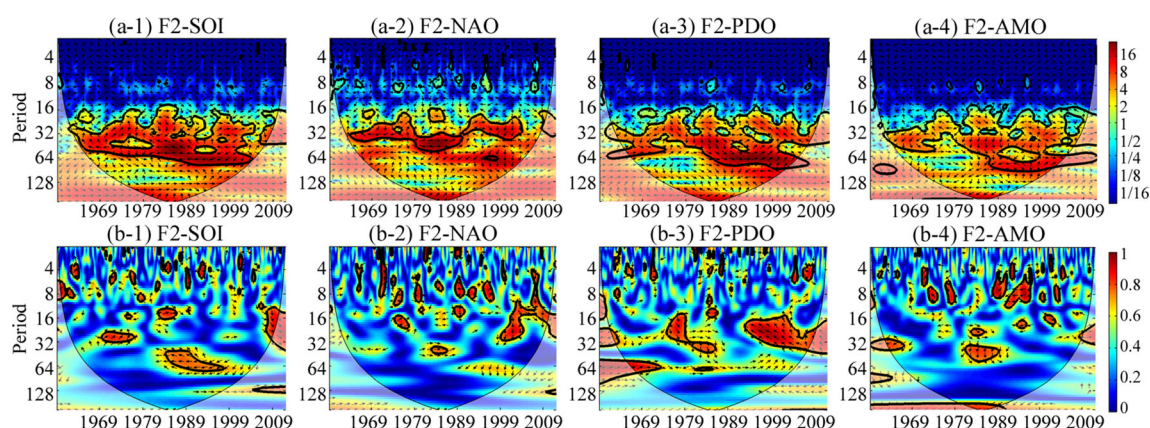


Fig. 8 **a** Cross wavelet power spectrum and **b** wavelet coherence between F2 score series of SPI₁₂ and climate indices (SOI, NAO, PDO, and AMO). The *thick black contours* depict the 5% significance level of

local power relative to red noise, and the cone of influence (COI) is shown as a *lighter shade*. *Right-pointing arrows* indicate that the two signals are in phase while *left-pointing arrows* are for anti-phase signals

50-month period in the 1980s. The significant correlation between the F3 score and PDO is found in the 28- to 43-month period from 1981 to 1996 and in the period of 75- to 128 months from 1990 to 2000. In addition, the AMO has significant influence on the sub-regional drought regime in the 28–43-month period during 1964–1974.

Generally, we can conclude that the global teleconnections (including ENSO, NAO, PDO and AMO) show strong influences on drought over the Luanhe River basin concentrated in the 16- to 64-month period, while considerable differences exist in the detailed links for the three distinct sub-regions. It is consistent with the potential periodicity observed for the regional drought based on CWT analysis, indicating that the large-scale climate patterns may play a crucial role in generating cyclical behavior of drought occurrences. It is also worth noting that PDO and AMO highlight the possible links to drought variability on decadal scales.

In addition, the teleconnections of these climatic indices with annual and seasonal droughts were investigated by applying the cross wavelet analysis. Corresponding to the

seasonal drought (represented by seasonal RPC score), the climate pattern considered in the analysis was defined as the average of its index values for the related months with the season. Table 3 summarizes the significant link between each climate index and the first three RPC (F1, F2, and F3) scores for annual and seasonal SPIs, according to the significant common power and wavelet coherence uncovered by using the XWT and WCO, respectively.

As shown in Table 3, the annual drought variability in R1 sub-region is significantly correlated with SOI in the 3- to 5-year period during 1969–1976, with PDO in 3.5- to 4.5-year period during 1970–1974, and with AMO in 2.5- to 5-year period during 1969–1974 and 1995–2002. AMO in the 9- to 10-year period also shows significant correlations with the sub-regional annual drought from 1973–1985. The annual drought in R2 sub-region exhibits a 2.5- to 3.5-year oscillation significantly linked to NAO during 1982–1987 and to AMO during 1966–1969. SOI and PDO with 3.5–6 year period signals have significant influence on this sub-regional drought during 1981–1998 and 1987–2001, respectively. In R3 sub-

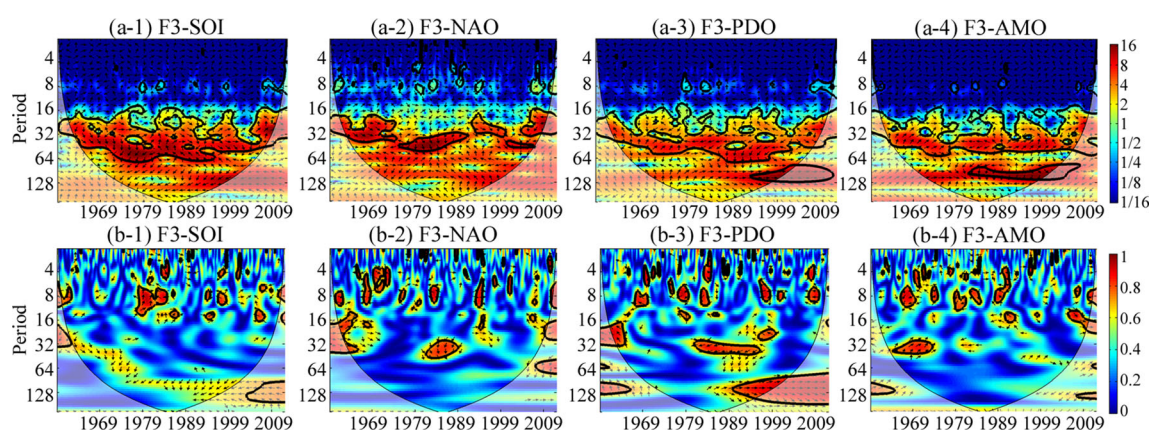


Fig. 9 **a** Cross wavelet power spectrum and **b** wavelet coherence between F3 score series of SPI₁₂ and climate indices (SOI, NAO, PDO, and AMO). The *thick black contours* depict the 5% significance level of

local power relative to red noise, and the cone of influence (COI) is shown as a *lighter shade*. *Right-pointing arrows* indicate that the two signals are in phase while *left-pointing arrows* are for anti-phase signals

Table 3 Summary of the significant link between each climate index and the first three RPC (F1, F2, and F3) scores for annual and seasonal SPIs based on the results of XWT and WCO

SPI	Climate index	F1 score		F2 score		F3 score	
		Time	Period (year)	Time	Period (year)	Time	Period (year)
	SOI	1969–1976	3–5	1981–1998	3.5–6	1976–1986	2–6
	NAO	–	–	1982–1987	2.5–3.5	1978–1986	2–6
	PDO	1970–1974	3.5–4.5	1987–2001	3.5–6	–	–
	AMO	1969–1974	2.5–5	1966–1969	2.5–3.5	–	–
Spring		1995–2002	2.5–5	–	–	–	–
		1973–1985	9–10	–	–	–	–
	SOI	1984–2002	3–6	1985–2000	3–6	1968–1984	12.5–15.5
	NAO	1987–1992	2–4	1990–2006	8–12.5	2001–2007	3–4
Summer		1996–2004	8–10	–	–	–	–
	PDO	1995–2006	7.5–10	1990–2004	8–11	1961–1992	12.5–18
	AMO	1984–1995	3–5	1984–2005	6–10	–	–
	SOI	1971–1982	4–6	1976–1988	2.5–5.5	1967–1977	3–5
Autumn		–	–	–	–	1994–2005	9–11
	NAO	1982–2005	5–7	1986–1997	5–7	–	–
	PDO	–	–	1977–1984	3–4	–	–
	AMO	–	–	1977–1993	8–11	1982–2010	7.5–13.5
Winter	SOI	1965–1972	2.5–4	1968–1982	3.5–5	1967–1973	2.5–5
		1969–2000	10–16.5	–	–	–	–
	NAO	1964–1979	2–4	2000–2010	3–5	–	–
		1973–1986	12.5–16.5	–	–	–	–
Winter	PDO	–	–	–	–	1995–2005	6.5–8.5
	AMO	–	1980–1990	7–10	–	–	–
	SOI	–	–	1968–1989	3.5–5	–	–
	NAO	1984–1989	2–3	1969–1983	5.5–9.5	1974–1980	6–8
		–	–	1980–1988	2–4	1994–2000	2–3
	PDO	2001–2010	8–11	–	–	–	–
	AMO	–	–	–	–	–	–

region, both SOI and NAO with 2–6 year period signals have significant associations with the annual drought during 1976–1986. These results may highlight the decisive role of the climate patterns in the periodical feature (2- to 6-year) of annual drought in the Luanhe River basin.

On the whole, all these climate patterns have significant influences on spring drought over the Luanhe River basin concentrated in the 2- to 6-year period and in the 8- to 10-year period. For the R3 sub-region, the impacted cycles related with both ENSO and PDO extend to 12 to 18 years, while the influence of AMO is observed to be in-apparent. As for summer drought, a significant correlation with SOI in the 3- to 5-year period is detected in all the sub-regions, and NAO, PDO, and AMO with various period signals are found to be remarkably correlative in the R2 sub-region. SOI and AMO also indicate significant links to the summer drought on a decadal scale (about 10-year period) in the R3 sub-region. The variability of autumn drought is significantly associated with SOI and NAO both in the 3- to 5-year period, generally across the whole basin. Meanwhile, these two indices in the 12- to 16-year period also show noteworthy relations with the autumn drought in the R1 sub-region. In addition, winter drought conditions over the basin are primarily dominated by NAO with 2–3 and 6–8-year period signals. SOI in the 3- to 5-year period and PDO in the 8- to 11-

year period highlight a significant correlation with the winter drought in the R2 sub-region and the R3 sub-region, respectively.

Although the cause of drought variability in the Luanhe River basin is controversial under a changing environment, several previous studies have already provided evidences for the significant effects of atmospheric teleconnections on hydrological processes and drought characteristics. However, there are still questions as to how the climate patterns affect the spatial and temporal structure of droughts, particularly interested in annual to decadal variations. In this study, the cross wavelet analysis was employed to reveal the possible link between large-scale climate anomalies and regional drought variability in the time-frequency domain. The related results can explain the different drought behaviors found in the three sub-regions to some extent and suggest that different physical mechanism maybe are acting on the sub-regional drought conditions at various time scales. Under the background of global warming, these possible links could provide guidance for policy makers in drought mitigation and adaptation strategies.

ENSO is the dominant coupled ocean-atmosphere mode of the tropical Pacific, and its remarkable effects on the occurrence and evolution of drought in northern China have been proven by several previous studies (e.g., Su and Li 2012; Ouyang et al. 2014). During the typical warm phase of

ENSO, drier surface conditions even severe drought events generally occur at high frequencies in North China (Lu et al. 2006; Su and Wang 2007). Chen and Shi (2003) found that autumn precipitation in China shows a fairly close relation with ENSO. The study of Luo (2000) indicated that the summer precipitation of North China is generally lower, possibly causing drought events in the developing stage of ENSO. Moreover, Li et al. (2015) developed a non-stationary distribution with climate indices as covariates for fitting 12-month cumulative precipitation over the Luanhe River basin and found that SOI might be one of the dominant causes for the non-stationary behavior of the precipitation observations. These conclusions confirmed our findings that there are quite strong associations between ENSO and drought conditions over the Luanhe River basin.

NAO is viewed as the dominant mode of winter atmospheric circulation across North Atlantic. Hurrell (1995 and 1996) and Hurrell and van Loon (1997) reported that NAO might make the greatest contribution to the temperature change in the Northern Hemisphere, and its variation could largely explain the warming occurred in Eurasia during the 1980s. Several studies have revealed the strong influence of NAO on the climate anomalies in China, especially on the winter climate (Wang and Shi 2001; Fu and Zeng 2005; Song et al. 2011). Wang and Shi (2001) discussed the relationship between NAO and winter climate in China, and they suggested that the larger values of NAO index are directly correlated with the higher temperature in winter across the northern part of North China. Wu and Huang (1999) also demonstrated the remarkable impact of winter NAO on the East Asia winter monsoon that directly affects the winter climate of the Luanhe River basin. In this study, the influence of NAO on winter droughts was found to be forceful across the Luanhe River basin. Consistency in the results of previous studies and ours strengthens the credibility of the predominant effect of NAO.

PDO is a pattern of climatic variability in the Pacific Ocean with a characteristic time scale of 20–30 years (Hare and Mantua 2001). Ouyang et al. (2014) investigated the impact of PDO on precipitation and streamflow in China during 1901–2009. Their results revealed that the PDO warm phase mainly decrease while the PDO cool phase increase the precipitation and streamflow in the majority of China, along with regional and seasonal differences. Ma and Shao (2006) found that PDO is closely correlated to dry/wet evolution of northern China and the correlation is particularly obvious in North China at inter-decadal scale, by using monthly precipitation and monthly mean air temperature data during 1901–2002. In addition, Ma (2007) also suggested that the warm phases of PDO commendably correspond to the drying period with less rainfall and high temperature in North China, most likely highlighting the leading role of PDO in the regional dry/wet variation at inter-decadal scale. A similar conclusion was reported by Zhu and Yang (2003). These previous findings

give confidence in our results, which pointed out the significant linkage of PDO to annual/seasonal droughts in the Luanhe River basin observed at inter-decadal scales.

AMO represents a climate oscillation in the North Atlantic with a period of 65–80 years (Kerr 2000). It has become a consensus that the warm phase AMO intensifies the East Asian summer monsoon but weakens the winter monsoon (Wang et al. 2009). Many previous studies demonstrated that the warm AMO phase plays a leading role in the substantial East Asian warming in the recent two decades (Li et al. 2009; Wang et al. 2010) and meanwhile favors warmer winters with enhanced precipitation in North China (Ma and Ren 2007; Li and Bates 2007). Wang et al. (2015b) used correlation analysis to evaluate the effects of ESON and AMO on hydrological drought in the Luanhe River basin, indicating a significant influence of AMO. These consistent evidences can well support our tentative conclusion that AMO shows significant influence on the drought variability of the Luanhe River basin especially on inter-decadal scales.

5 Conclusions

It is vital to understand the spatial and temporal variability of drought for better mitigation and adaptation strategies. Focusing on Luanhe River basin in this study, monthly precipitation data during the period of 1958–2011 were used, from 26 rain-gauging stations distributed uniformly over the basin. The spatial structures of drought were analyzed by applying the PCA to the SPI estimated on 3- and 12-month time scales, as well as annual and seasonal SPIs. Then, the Mann-Kendall trend test with the TFPW procedure and the Sen's slope estimator were used to detect the temporal tendency in drought, and the CWT was employed to identify the periodic features. Moreover, the possible relationships between global teleconnection patterns and sub-regional drought variability were recognized by means of the cross wavelet analysis. The main conclusions can be summarized as follows:

1. A well-defined spatial structure with three distinct sub-regions was achieved for the Luanhe River basin, namely the southeastern part, the middle part, and the northwestern part. Each sub-region has its individual temporal evolution of drought conditions, depending on different precipitation regimes.
2. Over the Luanhe River basin, results of MK and Sen's tests generally show evidences of a significant aggravating trend in summer drought and a prominent trend indicating drought mitigation in spring. At the annual scale, intensification of drought severity was detected across the basin overall. Moreover, the drought condition in the entire basin is subjected to a 16- to 64-month significant cycles over the past 53 years in terms of SPI₁₂. The

periodicity in the northwest is weaker as compared with that in the middle and southeast. The 2- to 6-year cycle is clear evident when concerned with annual and seasonal droughts.

- Based on the cross wavelet analysis, the significant influence of large-scale climate patterns (represented by ENSO, NAO, PDO, and AMO) on drought in the Luanhe River basin is concentrated in the 16- to 64-month period, possibly responsible for the physical cause of cyclic behaviors of the regional drought condition. The PDO and AMO with signals on decadal scales (around 128-month period) show noteworthy correlations with the drought variability.

The findings of this study will be useful for drought mitigation and water resource management at a sub-regional scale. However, the drought characteristics detected in this study are directly based on historical data. Under a continuously changing environment, it is uncertain how these characteristics will evolve in the future. Hence, as a future work, various climate scenarios and models will be developed to further examine the impacts of climate change on drought characteristics in the Luanhe River basin.

Acknowledgements This work was financially supported by the National Natural Science Foundation of China (No. 51479130). The authors thank the Hydrology and Water Resource Survey Bureau of Hebei Province for providing the observed precipitation data.

References

- Abramowitz M, Stegun IA (1965) Handbook of mathematical functions. Dover Publication, New York
- Afzal M, Mansell MG, Gagnon AS (2011) Trends and variability in daily precipitation in Scotland. *Procedia Environmental Science* 6:15–26
- Atta-ur-Rahman, Dawood, M., 2016. Spatio-statistical analysis of temperature fluctuation using Mann–Kendall and Sen’s slope approach. *Clim Dyn* doi:10.1007/s00382-016-3110-y.
- Barnston AG, Livezey RE (1987) Classification, seasonality and persistence of low-frequency atmospheric circulation patterns. *Mon Wea Rev* 115:1083–1126
- Bartlett MS (1954) A note on the multiplying factors for various χ^2 approximations. *J Roy Stat Soc B* 16(2):296–298
- Bonaccorso B, Bordi I, Cancelliere A (2003) Spatial variability of drought: an analysis of the SPI in Sicily. *Water Resour Manag* 17(4):273–296
- Bordi I, Fraedrich FW, Gerstengarbe FW, Werner C, Sutera A (2004) Spatio-temporal variability of dry and wet periods in eastern China. *Theor Appl Climatol* 77:125–138. doi:10.1007/s00704-003-0029-0
- Capra A, Scicolone B (2012) Spatiotemporal variability of drought on a short-medium time scale in the Calabria Region (Southern Italy). *Theor Appl Climatol* 110(3):471–488
- Chen Y, Shi N (2003) El Nino/ENSO and climatic anomaly in the autumn of China. *J Trop Meteorol* 19(2):137–146 (in Chinese)
- Chen F, Yuan YJ, Chen FH, Wei WS, Yu SL, Chen XJ, Fan ZA, Zhang RB, Zhang TW, Shang HM, Qin L (2013) A 426-year drought history for Western Tian Shan, Central Asia inferred from tree-rings and its linkages to the North Atlantic and Indo-West Pacific Oceans. *The Holocene* 23:1095–1104
- Corte-Real J, Qian B, Xu H (1998) Regional climate change in Portugal: precipitation variability associated with large-scale atmospheric circulation. *Int J Climatol* 18:619–635
- Da Silva RM, Santos CA, Moreira M, Corte-Real J, Silva VC, Medeiros IC (2015) Rainfall and river flow trends using Mann–Kendall and Sen’s slope estimator statistical tests in the Cobres River basin. *Nat Hazards* 77(2):1205–1221
- Edossa DC, Babel MS, Gupta AD (2010) Drought analysis in the Awash River basin. *Ethiopia Water Resour Manag* 24(7):1441–1460
- Enfield DB, Mestas-Nunez AM, Trimble PJ (2001) The Atlantic multidecadal oscillation and its relation to rainfall and river flow over the U.S. *Geophys Res Lett* 28:2077–2080
- Fu CB, Zeng ZM (2005) The relationship between winter North Atlantic Oscillation index and summer eastern China dryness/wetness index in recent 530a. *Chin Sci Bull* 50(14):1512–1522 (in Chinese)
- Gan TY (1998) Hydroclimatic trends and possible climatic warming in the Canadian prairies. *Water Resour Res* 34(11):3009–3015
- Gao YD (2012) Water demand predication and countermeasure study on sustainable utilization of water resources of the Luanhe River basin, Chengde City. *Northwest Hydropower* 02:6–13 (in Chinese)
- Ghil M, Allen MR, Dettinger MD, Ide K, Kondrashov D, Mann ME, Robertson AW, Saunders A, Tian Y, Varadi F, Yiou P (2002) Advanced spectral methods for climatic time series. *Rev Geophys* 40(1):1–41
- Gilbert RO (1987) Statistical methods for environmental pollution monitoring. Van Nostrand Reinhold Company, New York, pp 204–208
- Gocic M, Trajkovic S (2013) Analysis of changes in meteorological variables using MannKendall and Sen’s slope estimator statistical tests in Serbia. *Glob. Planet. Change* 100:172–182
- Gocic M, Trajkovic S (2014) Spatiotemporal characteristics of drought in Serbia. *J Hydrol* 510:110–123
- Grinsted A, Moore JC, Jevrejeva S (2004) Application of the cross wavelet transform and wavelet coherence to geophysical time series. *Nonlinear process. Geophys* 11(5/6):561–566
- Guttman NB (1997) Comparing the palmer drought index and the standardized precipitation index. *J Am Water Resour As* 34:113–121
- Hamed KH (2008) Trend detection in hydrologic data: the Mann–Kendall trend test under the scaling hypothesis. *J Hydrol* 349:350–363
- Hare, S.R., Mantua, N.J., 2001. An historical narrative on the Pacific Decadal Oscillation, interdecadal climate variability and ecosystem impacts, CIG Publication No. 160. University of Washington, Seattle, WA.
- Hayes M, Wilhite DA, Svodoba M, Vanyarkho O (1999) Monitoring the 1996 drought using the standardized precipitation index. *Bull Am Meteorol Soc* 80:429–438. doi:10.1175/1520-0477(1999)080<0429:MTDUTS>2.0.CO;2
- Heim RR (2002) A review of twentieth-century drought indices used in the United States. *Bull Am Meteorol Soc* 83(8):1149–1165
- Hosseinzadeh Talaee P, Tabari H, Sobhan Ardakani S (2014) Hydrological drought in the west of Iran and possible association with large-scale atmospheric circulation patterns. *Hydrol Process* 28(3):764–773
- Hotelling H (1933) Analysis of a complex of statistical variables into principal components. *Journal Educ Psychology* 24(417–441): 498–520
- Hurrell JW (1995) Decadal trends in the North Atlantic oscillation: regional temperatures and precipitation. *Science* 269(5224):676–679
- Hurrell JW (1996) Influence of variations in extratropical wintertime teleconnections on Northern Hemisphere temperature. *Geophys Res Lett* 23(6):665–668
- Hurrell JW, Van Loon H (1997) Decadal variations in climate association with the North Atlantic Oscillation. *Clim Chang* 36(3/4):301–326

- Jevrejeva S, Moore JC, Grinsted A (2003) Influence of the Arctic Oscillation and El Niño-Southern Oscillation (ENSO) on ice conditions in the Baltic Sea: the wavelet approach. *J Geophys Res Atmos* 108(D21):4677
- Kahya E, Demirel MC, Beg OA (2008) Hydrologic homogeneous regions using monthly streamflow in Turkey. *Earth Sci Res J* 12(2): 181–193
- Kaiser HF (1970) A second generation little jiffy. *Psychometrika* 35(4): 401–415
- Kao SC, Govindaraju RS (2010) A copula-based joint deficit index for droughts. *J Hydrol* 380(1):121–134
- Kendall MG (1975) Rank correlation methods. Griffin, London
- Kerr RA (2000) A North Atlantic climate pacemaker for the centuries. *Science* 288(5473):1984–1986
- Kisi O, Ay M (2014) Comparison of Mann–Kendall and innovative trend method for water quality parameters of the Kizilirmak River. *Turkey J Hydrol* 513:362–375
- Kousari MR, Ahani H, Hendi-zadeh R (2013) Temporal and spatial trend detection of maximum air temperature in Iran during 1960–2005. *Glob Planet Change* 111:97–110. doi:10.1016/j.gloplacha.2013.08.011
- Labat D (2005) Recent advances in wavelet analyses: part 1. A review of concepts. *J Hydrol* 314:275–288
- Labat D (2008) Wavelet analysis of the annual discharge records of the world's largest rivers. *Adv Water Resour* 31(1):109–117
- Labat D (2010) Cross wavelet analyses of annual continental freshwater discharge and selected climate indices. *J Hydrol* 385:269–278
- Labat D, Goddérís Y, Probst JL, Guyot JL (2004) Evidence for global runoff increase related to climate warming. *Adv Water Resour* 27(6):631–642
- Labat D, Ronchail J, Guyot JL (2005) Recent advances in wavelet analyses: part 2—Amazon, Parana, Orinoco and Congo discharges time scale variability. *J Hydrol* 314(1–4):289–311
- Lafreniere M, Sharp M (2003) Wavelet analysis of inter-annual variability in the runoff regimes of glacial and nival stream catchments, Bow Lake. *Alberta Hydrol Proc* 17:1093–1118
- Li SL, Bates GT (2007) Influence of the Atlantic multidecadal oscillation on the winter climate of East China. *Adv Atmos Sci* 24(1):126–135
- Li JZ, Feng P (2007) Runoff variations in the Luanhe river basin during 1956–2002. *J Geogr Sci* 17(3):339–350
- Li JZ, Zhou SH (2015) Quantifying the contribution of climate- and human-induced runoff decrease in the Luanhe river basin, China. *J Water Clim Change*. doi:10.2166/wcc.2015.041
- Li SY, Wang YM, Gao YQ (2009) A review of the researches on the Atlantic multidecadal oscillation (AMO) and its climate influence. *Trans Atmos Sci* 32(3):458–465 (in Chinese)
- Li S, Xiong LH, Dong LH, Zhang J (2013a) Effects of the Three Gorges Reservoir on the hydrological droughts at the downstream Yichang station during 2003–2011. *Hydrol Process* 27(26):3981–3993
- Li B, Su HB, Chen F, Li SG, Tian J, Qin YC, Zhang RH, Chen SH, Yang YM, Rong Y (2013b) The changing pattern of droughts in the Lancang River basin during 1960–2005. *Theor Appl Climatol* 111: 401–415
- Li JZ, Wang YX, Li SF, Hu R (2015) A nonstationary standardized precipitation index incorporating climate indices as covariates. *J Geophys Res Atmos* 120. doi:10.1002/2015JD023920
- Liu ZY, Zhou P, Zhang FQ, Liu X, Chen G (2013) Spatiotemporal characteristics of dryness/wetness conditions across Qinghai Province. *Northwest China Agr Forest Meteorol* 182–183:101–108
- Livada I, Assimakopoulos V (2007) Spatial and temporal analysis of drought in Greece using the standardized precipitation index (SPI). *Theor Appl Climatol* 89:143–153
- Lorenzo-Lacruz, J., Vicente-Serrano, S.M., López-Moreno, J.I., Beguería, S., García-Ruiz, J.M., Cuadrat, J.M., 2010. The impact of droughts and water management on various hydrological systems in the headwaters of the Tagus River (central Spain). *J Hydrol* 386, 13–26.
- Lu AG, Ge JQ, Pang DQ, He YQ, Pang HX (2006) Asynchronous response of droughts to ENSO in China. *J Claciol Geocryol* 28(4): 535–542 (in Chinese)
- Luo GY (2000) A general survey of the studies on El Niño and La Niña in China. *Sci Geogr Sin* 20(3):264–269 (in Chinese)
- Ma ZG (2007) Relationship between the Pacific Decade Oscillation (PDO) and the drying tendency in North China. *Chin Sci Bull* 52(10):1199–1206 (in Chinese)
- Ma ZG, Ren XB (2007) Drying trend over China from 1951 to 2006. *Adv Clim Change Res* 3(4):195–201 (in Chinese)
- Ma ZG, Shao LJ (2006) Relationship between dry/wet variation and the Pacific decade Oscillation (PDO) in northern China during the last 100 years. *Chinese Journal of Atmospheric Sciences* 30(3):464–474 (in Chinese)
- Ma H, Yang D, Tan SK, Gao B, Hu Q (2010) Impact of climate variability and human activity on streamflow decrease in the Miyun Reservoir catchment. *J Hydrol* 389(3):317–324
- Ma HJ, Yan DH, Weng BS, Fang HY, Shi XL (2013) Applicability of typical drought indexes in the Luanhe River basin. *Arid Zone Research* 30(4):728–734 (in Chinese)
- Mann HB (1945) Nonparametric tests against trend. *Econometrica* 13: 245–259
- Maraun D, Kurths J (2004) Cross wavelet analysis: significance testing and pitfalls. *Nonlinear Process Geophys* 11:505–514
- Martins DS, Raziei T, Paulo AA, Pereira LS (2012) Spatial and temporal variability of precipitation and drought in Portugal. *Nat Hazards Earth Syst Sci* 12:1493–1501
- McKee, T.B., Doesken, N.J., Kleist, J., 1993. The relationship of drought frequency and duration to time scales. In: 8th Conference on Applied Climatology, 17–22 January, Anaheim, California, pp. 179–184
- McKee TB, Doesken NJ, Kleist J (1995) Drought monitoring with multiple time scales, paper presented at 9th conference on applied climatology. American Meteorological Society, Dallas, Texas
- Mishra AK, Singh VP (2010) A review of drought concepts. *J Hydrol* 391(1–2):202–216
- Moreira EE, Martins DS, Pereira LS (2015) Assessing drought cycles in SPI time series using a Fourier analysis. *Nat Hazards Earth Syst Sci* 15:571–585
- Oglesby R, Feng S, Hu Q, Rowe C (2012) The role of the Atlantic Multidecadal Oscillation on medieval drought in North America: synthesizing results from proxy data and climate models. *Glob Planet Chang* 84:56–65
- Ouyang R, Liu W, Fu G, Liu C, Hu L, Wang H (2014) Linkages between ENSO/PDO signals and precipitation, streamflow in China during the last 100 years. *Hydrol Earth Syst Sci Discuss* 11(4):4235–4265
- Özger M, Mishra AK, Singh VP (2009) Low frequency drought variability associated with climate indices. *J Hydrol* 364(1):152–162
- Partal T, Kahya E (2006) Trend analysis in Turkish precipitation data. *Hydrol Process* 20:2011–2026
- Paulo AA, Pereira LS (2006) Drought concepts and characterization: comparing drought indices applied at local and regional scales. *Water Int* 31:37–49
- Paulo AA, Rosa RD, Pereira LS (2012) Climate trends and behaviour of drought indices based on precipitation and evapotranspiration in Portugal. *Nat Hazards Earth Syst Sci* 12(5):1481–1491
- Potop V, Soukup J (2009) Spatiotemporal characteristics of dryness and drought in the Republic of Moldova. *Theor Appl Climatol* 96(3): 305–318
- Raziei T, Bordi I, Pereira LS (2013) Regional drought modes in Iran using the SPI: the effect of time scale and spatial resolution. *Water Resour Manag* 27(6):1661–1674
- Rencher AC (1998) Multivariate statistical inference and applications. John Wiley & Sons, Inc

- Richman MB (1986) Rotation of principal components. *Int J Climatol* 6: 293–335
- Russo S, Dosio A, Sterl A, Barbosa P, Vogt J (2013) Projection of occurrence of extreme dry-wet years and seasons in Europe with stationary and nonstationary standardized precipitation indices. *J Geophys Res Atmos* 118:7628–7639
- Santos JF, Pulido-Calvo I, Portela MM (2010) Spatial and temporal variability of droughts in Portugal. *Water Resour Res* 46:W03503. doi:10.1029/2009WR008071
- Schaeffli B, Maraun D, Holschneider M (2007) What drives high flow events in the Swiss Alps? Recent developments in wavelet spectral analysis and their application to hydrology. *Adv Water Resour* 30(12):2511–2525
- Sen PK (1968) Estimates of the regression coefficient based on Kendall's tau. *J Am Stat Assoc* 63:1379–1389
- Sharma, S., 1996. Applied multivariate techniques. John Wiley & Sons pp.512
- Song J, Yang H, Li CY (2011) A further study of causes of the severe drought in Yunnan Province during the 2009/2010 winter. *Chinese Journal of Atmospheric Sciences* 35(6):1009–1019 (in Chinese)
- Su HX, Li GQ (2012) Low-frequency drought variability based on SPEI in association with climate indices in Beijing. *Acta Ecol Sin* 32(17): 5467–5475 (in Chinese)
- Su MF, Wang HJ (2007) Relationship and its instability of ENSO-Chinese variations in droughts and wet spells. *Sci China Ser D Earth Sci* 50(1):145–152 (in Chinese)
- Szalai, S., Szinell, C., Zoboki, J., 2000. Drought monitoring in Hungary. In: *Early Warning Systems for Drought Preparedness and Drought Management*, WMO, Geneva, pp.161–176
- Tabari H, Marofi S, Aeiini A, Hosseinzadeh Talaei P, Mohammadi K (2011) Trend analysis of reference evapotranspiration in the western half of Iran. *Agric For Meteorol* 151(2):128–136
- Torrence C, Compo GP (1998) A practical guide to wavelet analysis. *Bull Am Meteorol Soc* 79(1):61–78
- Torrence C, Webster P (1999) Interdecadal changes in the ENSO monsoon system. *J Clim* 12:2679–2690
- Ujeneza EL, Abiodun BJ (2015) Drought regimes in Southern Africa and how well GCMs simulate them. *Clim Dynam* 44:1595–1609
- Vargas WM, Naumann G, Minetti JL (2011) Dry spells in the River Plata Basin: an approximation of the diagnosis of droughts using daily data. *Theor Appl Climatol* 104:159–173
- Vicente-Serrano SM (2006) Differences in spatial patterns of drought on different time scales: an analysis of the Iberian Peninsula. *Water Resour Manag* 20:37–60
- Vicente-Serrano SM, López-Moreno JI (2005) Hydrological response to different time scales of climatological drought: an evaluation of the standardized precipitation index in a mountainous Mediterranean basin. *Hydrol Earth Syst Sci* 9:523–533
- Vicente-Serrano SM, Begueria S, Lorenzo-Lacruz J, Camarero JJ, Lopez-Moreno JI, Azorin-Molina C, Revuelto J, Moran-Tejeda E, Arturo Sanchez-Lorenzo A (2012) Performance of drought indices for ecological, agricultural, and hydrological applications. *Earth Interact* 16(10):1–27
- Vicente-Serrano SM, Chura O, López-Moreno JI, Azorin-Molina C, Sanchez-Lorenzo A, Aguilar E, Moran-Tejeda E, Trujillo F, Martínez R, Nieto JJ (2014) Spatio-temporal variability of droughts in Bolivia: 1955–2012. *Int J Climatol* DOI. doi:10.1002/joc.4190
- Wang YB, Shi N (2001) Relation of North Atlantic oscillation anomaly to China climate during 1951–1995. *Journal of Nanjing Institute of Meteorology* 24(3):315–322 (in Chinese)
- Wang YM, Li SL, Luo DH (2009) Seasonal response of Asian monsoonal climate to the Atlantic multidecadal oscillation. *J Geophys Res* 114: 1–15. doi:10.1029/2008JD010929
- Wang JS, Chen FH, Jin LY, Bai HZ (2010) Characteristics of the dry/wet trend over arid central Asia over the past 100 years. *Clim Res* 41(1):51–59
- Wang WG, Shao QX, Yang T, Peng SZ, Xing WQ, Sun FC, Luo YF (2013) Quantitative assessment of the impact of climate variability and human activities on runoff changes: a case study in four catchments of the Haihe River Basin. *China Hydrol Process* 27(8):1158–1174
- Wang HJ, Chen YN, Pan YP, Li WH (2015a) Spatial and temporal variability of drought in the arid region of China and its relationships to teleconnection indices. *J Hydrol* 523:283–296
- Wang YX, Li JZ, Feng P, Chen FL (2015a) Effects of large-scale climate patterns and human activities on hydrological drought: a case study in the Luanhe River basin. *China Nat Hazards* 76:1687–1710
- Wang YX, Li JZ, Feng P, Hu R (2015b) A time-dependent drought index for non-stationary precipitation series. *Water Resour Manag* 15:1–17
- Water Resources and Hydropower Planning And Design General Institute, MWR (2008) China drought strategy research. China Water Power Press, Beijing (in Chinese)
- Wei ZZ, Feng P (2011) Analysis of rainfall-runoff evolution characteristics in the Luanhe River basin based on variable fuzzy set theory. *J Hydraul Eng* 42(9):1051–1057 (in Chinese)
- Wen L, Rogers K, Ling J, Saintilan N (2011) The impacts of river regulation and water diversion on the hydrological drought characteristics in the Lower Murrumbidgee River. *Australia J Hydrol* 405(3): 382–391
- Wu BY, Huang RH (1999) Effects of the extremes in the North Atlantic Oscillation on East Asia winter monsoon. *Chinese Journal of Atmospheric Sciences* 23(6):641–651 (in Chinese)
- Wu H, Soh LK, Samal A, Chen XH (2008) Trend analysis of streamflow drought events in Nebraska. *Water Resour Manag* 22(2):145–164
- Yang ZY, Yuan Z, Fang HY, Yan DH (2013) Study on the characteristic of multiply events of drought and flood probability in Luanhe River basin based on copula. *J Hydraul Eng* 44(5):556–561 (in Chinese)
- Yeh CF, Wang J, Yeh HF, Lee CH (2015) Spatial and temporal streamflow trends in northern Taiwan. *Water* 7:634–651. doi:10.3390/w7020634
- Yin Y, Xu Y, Chen Y (2009) Relationship between flood/drought disasters and ENSO from 1857 to 2003 in the Taihu Lake basin. *China Quatern Int* 208(1):93–101
- Yue S, Pilon P, Phinney B, Cavadias G (2002) The influence of autocorrelation on the ability to detect trend in hydrological series. *Hydrol Process* 16:1807–1829
- Zhang J, Li DL, Li L, Deng WT (2013) Decadal variability of droughts and floods in the Yellow River basin during the last five centuries and relations with the North Atlantic SST. *Int J Climatol* 33(15): 3217–3228
- Zhu YM, Yang XQ (2003) Relationships between Pacific Decadal Oscillation (PDO) and climate variabilities in China. *Acta Meteorologica Sinica* 61(6):641–665 (in Chinese)